

A Versatile Collage Visualization Technique

Zhenyu Wang, Daniel Cohen-Or and Min Lu

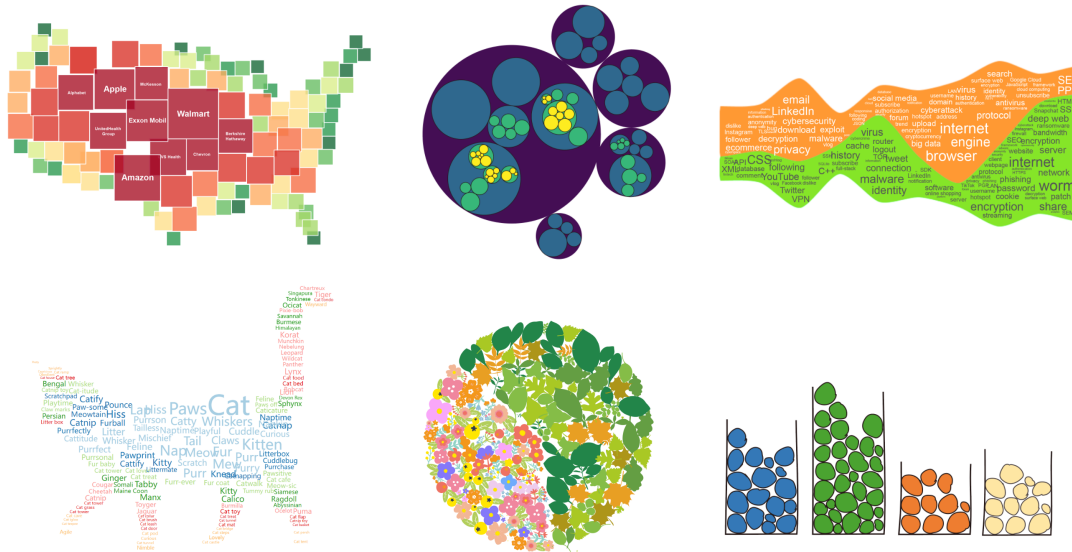


Fig. 1: Visualization created by our shape collage technique, from left to right: (top) square map, circular packing diagram, text themeriver, (bottom) word cloud, pie chart, and bubble barcharts.

Abstract— Collage techniques are commonly used in visualization to organize a collection of geometric shapes, facilitating the representation of visual features holistically, as seen in word clouds or circular packing diagrams. Typically, packing methods rely on object-space optimization techniques, which often necessitate customizing the optimization process to suit the complexity of geometric primitives and the specific application requirements. In this paper, we introduce a versatile image-space collage technique designed to pack geometric elements into a given shape. Leveraging a differential renderer and image-space losses, our optimization process is highly efficient and can easily accommodate various loss functions. We demonstrate the diverse visual expressiveness of our approach across various visualization applications. The evaluation confirmed the benefits of our method in terms of both visual quality and time performance. The project page is <https://szuviz.github.io/pixel-space-collage-technique/>.

Index Terms—Packing Diagram, Optimization, Differential Rendering.

1 INTRODUCTION

Assembling and collaging geometric elements to encapsulate visual features, provide a unified representation and have been instrumental in creating intriguing visualizations and artworks. Word clouds, or its variant known as wordles, are prime examples of this, where words are packed into a compact region to offer an engaging overview of texts [29]. Similarly, circular packing diagrams strategically fill a figure with circles to visually express the thematic topic [31].

Despite their popularity across various fields, the task of packing elements into given regions presents significant challenges. Numerous techniques have been proposed to address this task, with the majority

of existing shape collage methodologies concentrating on object-space optimization [14] [32]. To measure the fit between geometric objects, sophisticated geometric descriptors and loss functions are often tailored to specific types of geometric shapes.

However, such geometric object-based collage techniques come with several limitations. First, placement optimization in one application can hardly be applied to another. For instance, a technique that excels in packing rectangles [10] may not yield the same results when used to arrange words in a word cloud, owing to the significant differences in shape characteristics and layout requirements. Second, various geometric descriptors are required to capture geometric properties, particularly when dealing with complex or irregular shapes [28]. The huge searching space defined by object-based descriptors would impede the efficient identification of suitable docking locations for shapes. Third, the geometric shapes and the collage boundary they form can be subject to certain limitations in geometric optimization. For instance, some studies necessitate the use of geometric shapes with curvature and are unable to handle open shapes [14]. Some research efforts are constrained to fitting shapes within convex boundaries [32].

In this work, we advocate a paradigm shift in shape collage techniques. We propose transitioning the geometric packing optimization from the object space to the image space. The key idea is to leverage the power of differential rendering [18], a process that back propagates gradients for image pixels with respect to parameters of geometric

- Zhenyu Wang and Min Lu are with the School of Architecture and Urban Planning, Shenzhen University, Shenzhen, China. E-mail: yu2058724151@gmail.com, lumin.vis@gmail.com
- Daniel Cohen-Or is with the School of Computer Science, Tel Aviv University, Tel Aviv, Israel. E-mail: cohenor@gmail.com.
- Min Lu is the corresponding author of this work.

Manuscript received xx xxx. 201x; accepted xx xxx. 201x. Date of Publication xx xxx. 201x; date of current version xx xxx. 201x. For information on obtaining reprints of this article, please send e-mail to: reprints@ieee.org. Digital Object Identifier: xx.xxx/TVCG.201x.xxxxxxx

objects, to effectively steer the optimization process in the image space.

The core premise of our technique lies in its ability to harness the inherent advantages of image-space optimization. This includes its high efficiency, flexibility to accommodate powerful image-based loss functions and friendly accessibility to state-of-the-art image generative models. As shown in Figure 1, with varied geometric primitives and loss functions, our shape collage technique can generate a range of diverse visualizations. In the evaluation, our collage method is tested over a set of examples and the result supports its efficacy in time cost and data encoding fidelity.

2 RELATED WORK

This section explores research related to collage techniques, including text filling and graphic collage.

2.1 Text Filling

Considerable research has focused on arranging words to create text-based visualizations or word art. Word clouds, popular for visually representing words in a compact layout, have been extensively studied [5] [25] [29]. Tools such as Wordle [22] help with the easy creation of word clouds. Cui et al. [3] proposed a dynamic force-directed model for word cloud layout, which preserves semantic context over time. Wu et al. [33] utilized seam carving to optimize word cloud layouts. Beyond traditional word clouds, researchers have explored filling words within specific shapes. Paulovich et al. [24] introduced a cutting-stock optimization method that optimizes the arrangement of words to maximize space utilization within shapes. ShapeWordle [32] took a different approach by utilizing the Archimedean spiral to accommodate irregular shapes, resulting in visually appealing word cloud compositions. MetroWordle [17] combined word clouds with maps, incorporating collision detection for geotags. Chi et al. [2] presented temporally morphable word cloud technology that allows word clouds to undergo smooth shape transformations over time. Xie et al. [34] proposed animating word cloud for emotional expression.

Some other works support interactive word cloud customization. For example, Koh et al. [13] introduced an interactive interface to facilitate user-driven word manipulation within word clouds. Jo et al. [12] introduced WordPlus, which expands the interaction of Wordle by incorporating pen and touch interactions. Additionally, Surazhsky et al. [27] proposed a method for text layout on 3D objects. Maharik et al. [21] used streamline-based techniques to arrange words artistically. Zhang et al. [37] introduced a word arrangement method that arranges theme-related words at the salient areas. Xu et al. [36] introduced a tone-based ASCII art generation method.

Unlike object arrangement guided by space-filling curves or collision detection, our framework utilizes image-based loss for flexible word fitting, accommodating loose compositions like force-attracted filling in a non-closed constrained boundary.

2.2 Graphic Collage

Collages composed of closed shapes, like circles and icons, convey individual information while communicating an overall message. Packing objects into a container is a classic optimization problem, with numerous works addressing visualization and graphic design applications. Circular packing, exemplified by the work of Wang et al. [31], is a common paradigm, with new circles added to the outer periphery of existing ones. Several variations of packing have been developed, such as single-axis packing [20] [38]. Other techniques, like those by Itoh et al. [10], utilize force-directed layouts or hierarchical packing algorithms. Irregular shapes have also been considered, with methods like arclength descriptor matching [14] and autocompleteness-based optimization [6]. Calligraphic packing, employed for letter composition, has been explored by Xu et al. [35] and enhanced for legibility by Zou et al. [39].

Another related research topic is image collection or photo collage, in which the core task is to select a subset of photos to compose a collage that best represents the entire set. Many photo collage approaches have been proposed over decades [30] [26]. Goferman et al. [4] merged parts of photo into one whole image. Huang et al. [7] matched multiple

cutouts from the Internet to compose a thematic figure. Liu et al. [19] extracted salient regions and proposed a correlation-preserved photo collage. Pan et al. [23] presented a content-based visual summarization technique for image collections. More recently, instead of matching existing photos, Lee et al. [16] generated collage artwork via reinforcement learning, based on a given target image and materials. The typical idea is to model the part of each photo in a collage with geometric parameters, and then cast the photo collage into a complicated optimization problem over hundreds of parameters, with scores such as diversity, aesthetics, etc.

Existing methods propose complex geometric constraints or match objectives within the geometry space to facilitate shape or photo coupling. We take a different approach, exploring image space packing, avoiding the need for complex geometric computation and the use of task-specific descriptors. Our approach is highly generalizable, in the sense it can easily be adapted for a variety of applications.

3 PRELIMINARIES

In this section, we introduce two fundamental concepts, vector primitives and differential rendering, to facilitate the understanding of our method.

3.1 Vector Primitives

Vector graphics (i.e., SVG) use mathematical descriptions such as circles and paths to represent images in a resolution-independent manner. The majority of visualizations are created in the format of vector graphics, programming toolkits such as D3.js [1]. In a vectorized visualization, each data item can be described as one or a set of *vector primitives*. Taking the circular packing diagram as an example, each data item is presented by a vector primitive of a circle. In our approach, these primitives can take on arbitrary shapes and can be mixed up and optimized together. Therefore, we use a uniform format to represent primitives of any shape. A vector primitive is composed of linear, quadratic, or cubic segments. Each segment is further defined by a set of *control points*. As such, each primitive can be represented by a set of control points $\{(p_x, p_y)\}_{i=1}^m$, where m denotes the total number of control points.

3.2 Differential Rendering

Rasterization can be considered as a mapping (called scene function) from the vector graphics to a 2D pixel grid, denoted as $f(x, y; \Theta)$, where (x, y) is the position of pixel in the 2D grid, and Θ is the parameters of vector graphics. Differential rendering is a special rasterization, which renders vector graphics as images, while also allowing for the backpropagation of gradients. That is, in differential rendering, the scene function f is differentiated in terms of the parameters Θ . There is an observation that colors of pixels become continuous after anti-aliasing techniques, which prefilter f over a band-limited convolution kernel with area A [18]:

$$I(x, y) = \iint_A k(u, v) f(x - u, y - v; \Theta) du dv. \quad (1)$$

Considering there is no closed-form solution to compute $I(x, y)$, in this work, we use the anti-aliasing implementations proposed by Li et al. [18], which can compute the pixel integral I and its derivatives $\frac{\partial I}{\partial \Theta}$.

4 IMAGE-SPACE COLLAGE

In this section, we present our image-space collage methodology, discussing its primary components such as primitive initialization, geometric transformation, and the associated loss functions.

Figure 2 illustrates the framework of our method. Initially, vector primitives, which represent the data, are arranged in a specific initial layout (shall be introduced in Section 4.2). These vector primitives are then rasterized into an image through differential rendering. In this way, we cast the collage optimization problem into the image space, to minimize the rendering loss. Guided by the *target image* in which the collage is fit, a set of image-based loss functions (discussed in Section 4.3) are computed and back-propagated to a geometric

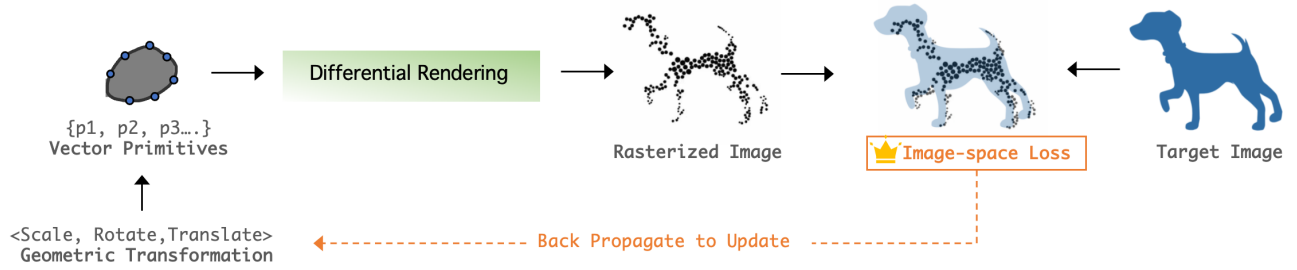


Fig. 2: Image-space Collage Framework: taking the initialized vector primitives as input, image-space losses are calculated between the rasterized image and the target image. These losses are used to update the parameters in the geometric transformation, which in turn updates the vector primitives.

transformation component. Following an update via gradient descent, the parameters within the geometric transformation are optimized to minimize the loss. Subsequently, we apply the updated geometric transformation to the vector primitives. The framework then continues to iterate until a state of minimal loss is attained. The decision to update the geometric transformation, rather than directly modifying the vector primitives, is to maintain the fidelity of data representation in visualization. More details about the geometric transformation process shall be provided in Section 4.1.

4.1 Geometric Transformation

In collage data visualization, visual primitives encode data via non-positional visual channels such as shape, size, height, or width. It is important to guarantee data encoding fidelity when optimizing the collage visualization. A direct update on the control points of visual primitives in the optimization is unstable, since it is difficult to maintain the original shape or size.

To ensure the positional invariance of visual primitives during the optimization, we introduce geometric transformation into the framework, which includes three operations (i.e., scaling, translation, and rotation) to transform each visual primitive. For each primitive P_i , its geometric transformation consist of scaling factor s_i , rotation angle α_i , and translation offset $(t_x, t_y)_i$. During the backward propagation process, the control points of primitives remain fixed, and optimization is performed on the parameters related to geometric transformation. With the new geometric transformation, visual primitives are updated for the next iteration.

4.2 Position Initialization

The initial positioning of visual primitives plays a crucial role in both optimization effectiveness and quality. When primitives are initialized either outside the target shape or at its border, they may be pushed outside the shape due to the *primitive overlap loss*. Once a primitive completely exits the target shape, it becomes challenging to trace it back solely with loss functions that assess how well the primitives fit within the shape. Escaping primitives can be attracted to moving back into the shape by introducing some distance loss functions, however, this would inevitably increase computational complexity and require more iterations. Similarly, if the initialization positions of primitives are not sufficiently uniformly distributed over the shape, more iterations would be needed, compared to the well-distributed ones.

Proper initial placement of vector primitives facilitates the optimization. In this work, we adopt the Medial Axis Transform (MAT) [15], which can effectively capture the primary contour and shape of objects. By applying the MAT algorithm, we obtain the coordinates of all points on the medial axis and their distances to the nearest boundary point (i.e., the medial width). As Figure 3 shows, with MAT, an area with a larger medial width provides more space to accommodate larger primitives, and vice versa. Given this, we distribute visual primitives along the medial axis, employing a strategy that positions larger primitives at medial points with a greater medial width. By utilizing the coordinates

of the medial axis and the medial width for initialization, shape primitives can be distributed more evenly at the skeletal positions inside the shape according to the weights, reducing the number of iterations and improving the filling effect.

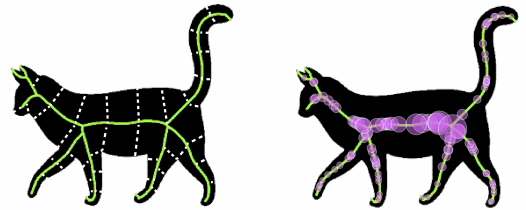


Fig. 3: MAT-based Position Initialization: with the detected medial axes and their nearest associated widths to the boundary (left), visual primitives are initialized in the way that larger primitives are placed on axes with larger medial widths.

4.3 Loss Functions

In our framework, we employ a variety of image-space loss functions to optimize the arrangement of visual primitives within a target shape. These functions allow to better fit the primitives to the target, avoid significant overlap among them, and simulate the mutual attraction effect between objects.

Boundary Fitness. To better fit the primitives to the target shape, we enhance our image-domain loss function with a spatial weighting scheme for iterative optimization of vector primitives. After differentiable rendering, the vector primitives yield a rendered image $\hat{I} \in \mathbb{R}^{w \times h \times 3}$. Given the target image $I \in \mathbb{R}^{w \times h \times 3}$, and a weight matrix $W \in \mathbb{R}^{w \times h}$ where W_{ij} is small if the pixel (i, j) is within the target shape and large if it is outside, we calculate the weighted Mean Squared Error (WMSE) between I and the target image \hat{I} , as following:

$$\mathcal{L}_{wmse} = \frac{1}{w \cdot h} \sum_{i=1}^w \sum_{j=1}^h W_{ij} \cdot \|\hat{I}_{ij} - I_{ij}\|^2, \quad (2)$$

where i is the index of the pixel. The objective of minimizing the MSE loss is to reduce the discrepancy between the rendered image \hat{I} and the target image I . This process fosters ideal placement of primitives inside the target shape and imposes penalties on primitives that extend beyond the target shape’s boundaries.

Primitive Overlap. While the loss \mathcal{L}_{mse} aids in aligning the rendered image with the target, it alone may not be sufficient. There is a possibility that primitives might overlap each other merely to fit within the target shape. This overlap could lead to less accurate representations. Therefore, to mitigate this issue, it becomes necessary to introduce an additional loss function specifically designed to penalize overlapping

among primitives. We introduce the mutual overlap among primitives to get another loss component:

$$\mathcal{L}_{ol} = ReLU\left(\sum_{i=0}^n A_i - \hat{A}\right), \quad (3)$$

where i is the index of the primitive, A_i is the area of the i^{th} primitive, and \hat{A} is the area of the aggregated shape rendered by all primitives. In practice, the area A_i of a primitive can be calculated by multiplying its initial area by the of its scaling factor s_i .

Data Fidelity. In the context of data visualization, it is crucial to maintain data fidelity across non-position visual channels. This means that transformations applied to visual primitives (i.e., scaling, translation, and rotation) should not result in loss of data fidelity. In our framework, there are two strategies to ensure data encoding fidelity. One is to set the scale in geometric transformation as a uniform global value, which will guarantee no distortion in visual encoding. The other strategy is individual scaling for each primitive, instead of applying a global scaling to all primitives. This decision is driven by the observation that global scaling induces changes in every primitive during each iteration, which could lead to instability in the optimization process. The constant shift and fluctuation of primitives under global scaling make it challenging to achieve stable and consistent optimization. To mitigate this, we employ individual scaling that allows us to adjust the size of each primitive independently, yet altering the size of individual primitive. To maintain overall coherence and to ensure that the primitives eventually conform to a unified global scale, we incorporate a *Data Fidelity Loss* function. Given the original primitive sizes $S_{orig} = \{s_{orig,i}\}_{i=1}^n$ and updated primitive sizes $S_{upd} = \{s_{upd,i}\}_{i=1}^n$, this loss function uses their cosine similarity as a measure:

$$\mathcal{L}_{fi} = 1 - \frac{S_{orig} \cdot S_{upd}}{\|S_{orig}\|_2 \cdot \|S_{upd}\|_2}, \quad (4)$$

where \cdot denotes the dot product, and $\|\cdot\|_2$ denotes the L2 norm (Euclidean norm). This function acts as a constraint, guiding the primitives to gradually align with a global scale as the optimization progresses.

Force Attraction. Visual primitives attracted towards certain points or direction creates intriguing visual effects in collage visualization [8]. Our framework introduces a *Attracting Loss* to accommodate this visual effect. Given an attracting point (r_x, r_y) , the attraction effect can be quantified by calculating the Euclidean distance between the distance of the centroid point of each visual primitive (c_{xi}, c_{yi}) and attracting point:

$$\mathcal{L}_d = \sum_{i=0}^n \sqrt{(c_{xi} - r_x)^2 + (c_{yi} - r_y)^2}, \quad (5)$$

where the centroid (c_{xi}, c_{yi}) of a primitive can be computed by offsetting its initial centroid point by the of the translation $(t_x, t_y)_i$ in the geometric transformation. Note this loss serves as an additional term in the optimization process to simulate the point attraction effect. Consequently, we can effectively implement force attraction effects in visualization tasks, thereby enriching the visualization results and enhancing visual impacts.

The overall loss function is then given by:

$$\mathcal{L}_{total} = \mathcal{L}_{wmse} + \beta \mathcal{L}_{ol} + \gamma \mathcal{L}_{fi} + \delta \mathcal{L}_d. \quad (6)$$

The coefficients β , γ and δ are the weights assigned to loss terms, determining their relative importance in the optimization process. By tuning these weights, we can prioritize certain aspects of the visualization over others, depending on the specific requirements of the task at hand.

5 EXAMPLES

In this section, we present our method’s capabilities in visualizing data at different levels. From conventional visualizations, our approach offers a versatile toolkit for generating visually compelling visualizations that cater to various needs and preferences.

5.1 Conventional Visualization

In this part, we present a set of conventional visualizations that effectively showcase the application of our method in visualizing real-world datasets. These visualizations serve as examples to demonstrate the effectiveness and reliability of our approach.

Figure 1 gives six conventional visualizations created using our image-space collage technique for real-world datasets. In the following part, we explain the configuration details of visual primitives and loss functions employed in each visualization.

Square Map In the left-top of Figure 1, we utilized a rectangular packing diagram to visualize the *top 100 companies in the United States based on their revenue data in 2023*. Each company is represented by a square and the size of the square corresponding to its yearly revenue. To ensure accurate representation, we employed the loss of data fidelity \mathcal{L}_{fi} to rigorously constrain the size of squares to match the revenue of each company. Taking the border of the United States as the target boundary, we successfully packed the squares with little overlap, resulting in a visually pleasing layout that resembles the shape of the United States. This approach effectively showcases the relative sizes of the companies while maintaining a cohesive and aesthetically pleasing visualization.

Circular Hierarchy Diagram The second example in upper row of Figure 1 is a circular packing diagram created to show the *hierarchical organization of a local university*. There are five schools within the university, each of which leads a tree structure of specific departments and laboratories. The size of the leaf circle is constrained by data fidelity loss \mathcal{L}_{fi} , to faithfully encode the popularity. Our college technique packs circles layer by layer in bottom-up manner. At each packing level, a force-attracting point is set at the centroid of the set of circles, utilizing the force attraction loss \mathcal{L}_d to attract the circles towards the center. As progressed to higher levels, new circles were created to enclose the previously placed circles. This iterative process continues until the whole hierarchy is covered.

Text ThemeRiver The third example of Figure 1 is a text themeriver that embeds *technology keywords in the client-server architecture*. The font size of the keyword represents its frequency. Taking the ribbons as the constrained boundaries for the two components, our technique takes the boundary boxes of words as visual primitives. To accomplish a compact layout, we combine two loss functions of boundary fitness \mathcal{L}_{wmse} and primitive overlap \mathcal{L}_{ol} . The boundary fitness loss function ensures that the words align well with the boundaries, while the primitive overlap loss function minimizes any excessive overlapping between words. By employing these techniques, the text themeriver enables practitioners to gain insights into the most prominent and trending topics within the field.

Word Cloud The bottom-left shows a word cloud about *cat’s facts*. Given a cat silhouette as the target boundary, keywords in different sizes are input as visual primitives to form a collage. Similar to text themeriver, boundary fitness \mathcal{L}_{wmse} and primitive overlap \mathcal{L}_{ol} are used during the packing.

Pie Chart In the bottom-middle, a pie chart showing *the percentage of flowering period* is created by flower and leaf icons. Although the icons are sophisticated, our collage techniques can fit them well with the loss functions of boundary fitness \mathcal{L}_{wmse} and primitive overlap \mathcal{L}_{ol} .

Bubble Barchart In the last example of Figure 1, we created the bubble barchart to represent *the sugar content of different fruit varieties in three categories*. The size of each bubble corresponds to the sugar content of a fruit variety, constrained by the data fidelity loss \mathcal{L}_{fi} . In each category, we used the rectangular bar as the constrained shape and enhanced the visualization by adding the attracting point below the bar, to simulate the effect of force attraction in the optimization. As seen in the example in Figure 1, this arrangement vividly captures the visual sensation of force attraction.

5.2 Illustrative Visualization

In this part, we delve into the realm of illustrative visualization, in which the emphasis is on creating visually appealing and memorable visuals that effectively communicate the main message or story behind the data. Illustrative visualization has been challenging to create. However, with

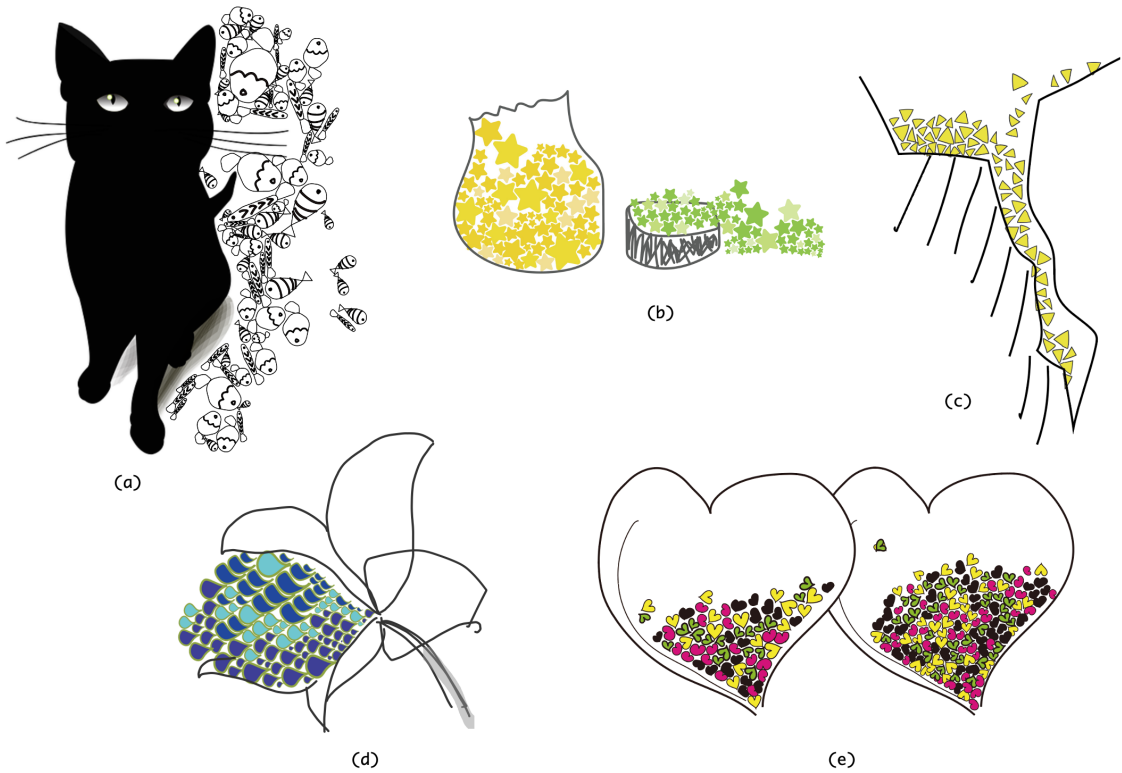


Fig. 4: Illustrative Visualization: by placing attracting points in different locations, visual effects that simulate the force of attraction can be achieved.

our method, we show how illustrative visualizations can now be easily generated.

Hand-drawn Illustrations Due to transforming the optimization process into the image space, our collage method eliminates the need to work with complex geometric descriptors for the optimization. This allows us to handle hand-drawn graphics more easily and effectively. As shown in the 'cat and fish' example (Figure 4(a)), an attracting point is introduced on the left of 'cat'. Using the right boundary of the cat to constrain the layout, fishes drawn in sketchy style are placed in a visually intriguing layout. By adding the *force attraction* loss (\mathcal{L}_d), our method can effectively stimulate force-attracted layouts in visualization. In the 'jars of stars' example (Figure 4(b)), by taking the 'jar' as the constrained boundary, we added an attracting point below the 'jar'. Stars are packed within the jar, replicating the visual effect of force attraction. In Figure 4(c), we added an attraction point below the 'rift valley', which effectively lead triangles into the valley. In Figure 4(d), we fit the data as part of the flower. Figure 4(e) shows two hand-drawn heart shapes containing different numbers of visual primitives, in which we want to show the potential of illustrative visualization for quantitative tasks, such as comparison.

Mosaic-style Illustration Mosaic-style visualization or artworks can be created by fitting visual primitives into shapes. Figure 5(a-c) shows several word clouds generated using our method. Taking the boundary boxes of words as the visual primitives, we combined the loss functions of *boundary fitness* \mathcal{L}_{wmse} and *primitive overlap* \mathcal{L}_{ol} to make a compact visual packing of words. Our methodology can effectively handle shapes with holes, as demonstrated by the examples of the seahorse (Figure 5(a)) and the '@' shape (Figure 5(c)). Additionally, our method excels at fitting words into different areas within a shape, as illustrated by the bird example in Figure 5(c). It can seamlessly accommodate words in narrow shapes like the bird's head and tail, as well as round shapes like the bird's belly, resulting in visually appealing word visualizations.

In Figure 5(d-f), we demonstrate the versatility of our packing al-

gorithm with regular shapes such as circles and triangles within constrained boundaries. Similar to word clouds, various shapes can be filled by various visual primitives, with the loss combination of *boundary fitness* \mathcal{L}_{wmse} and *primitive overlap* \mathcal{L}_{ol} . For example, in Figure 5(d), with presence of a 'red heart' shaped obstruction within the robot boundary, circles can be successfully optimized in the remaining space. Also, visual primitives constrained in isolated boundaries can be trained simultaneously, like the 'wheel' and 'car body' in the 'taxi' example (Figure 5(f)). Moreover, shapes can be fit into curvy boundaries as shown in the example of 'two wine cups' in Figure 5(e).

We also show more examples dealing with sophisticated vector icons to generate collages. Figure 5(g-k) shows four icon collages. As can be seen, even with sophisticated icons, our method fits them well within constrained boundaries both convex and concave shapes, such as the shape of a 'fork and spoon' in the left-bottom example. Without the necessity for complex geometric feature descriptors, our approach can effectively pair and align disparate shapes within a unified spatial configuration.

6 EVALUATION

We conducted two comprehensive experiments to evaluate the performance of our method from two key aspects: computational efficiency and data encoding fidelity. In the first user study on computational efficiency, we measured the time consumption of our technique. In the second study on data encoding fidelity, we examined how well our method preserves the original data throughout the collage creation process.

6.1 Computational Efficiency

To assess the computational consumption of our method, we conducted tests across *seven primitive scales* (i.e., different numbers of visual primitives, including 50, 100, 200, 400, 600, 800, and 1000.) We also considered *two levels of primitive complexity*, squares and irregular shapes, for low and high complexity, respectively. Given the same

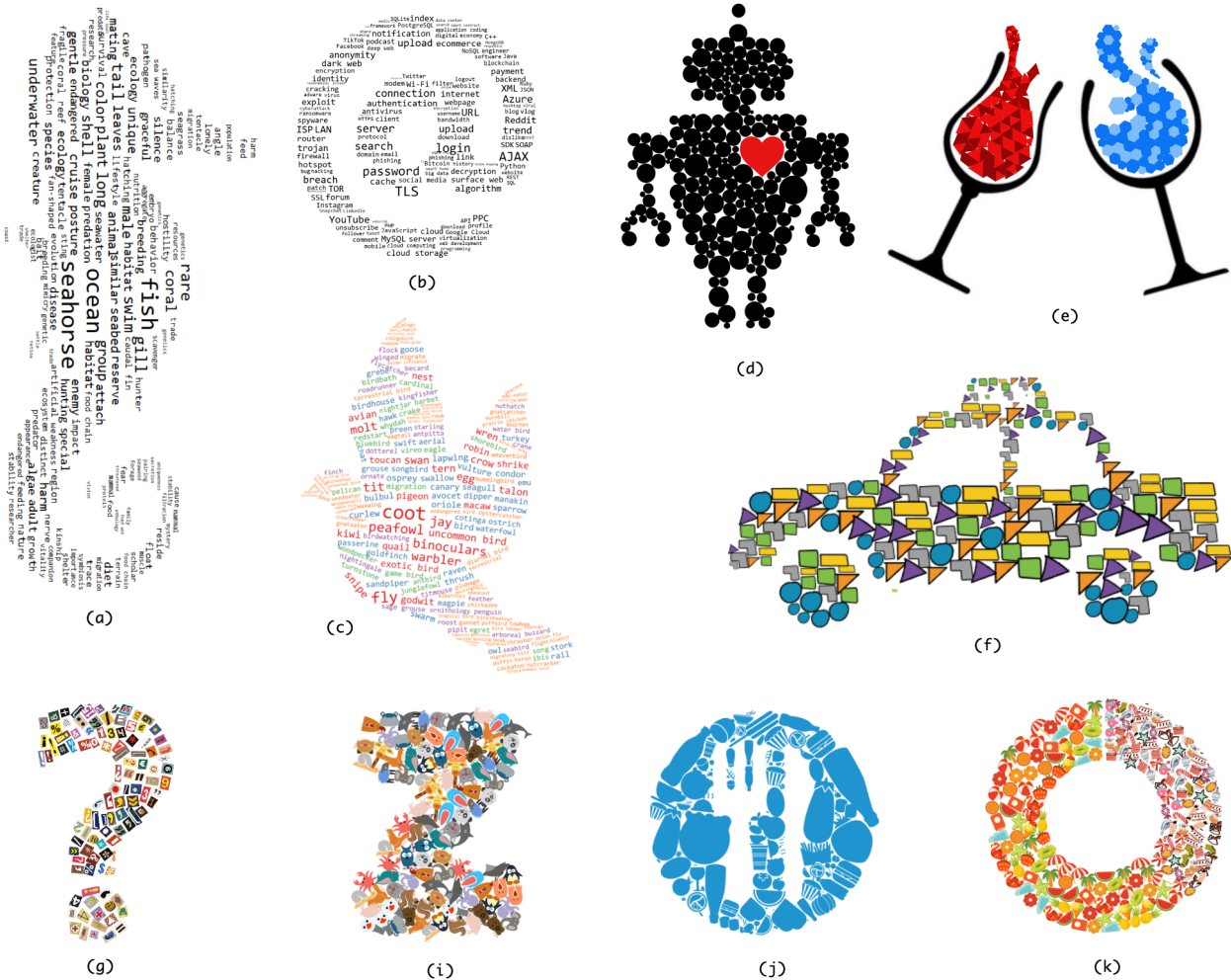


Fig. 5: Packing diagrams of words and shapes generated by our technique: (a-c) word clouds, (d-f) regular shapes, (g-k) irregular icons.

fitting boundary, our objective was to measure the average time cost per epoch and the number of epochs needed to achieve convergence to an overall low loss, and scalability in terms of primitive scale and complexity. By systematically varying these two parameters, we aimed to gain insights into the computational efficiency and convergence characteristics of our approach.

Time Cost We measured the time cost required for each epoch across different numbers of visual primitives and complexity levels, as shown in Table 1. From the table, we can draw the following conclusions: (1) *Effect of Primitive Scales*: As the number of primitives increases, the average time cost per epoch also tends to increase. This suggests that the computational effort required by the method grows as the complexity of the scene represented by the primitives becomes more intricate. (2) *Effect of Primitive Complexity*: Comparing the low and high primitive complexities, we observe that processing primitives with higher complexity result in longer average time costs per epoch. This indicates that handling complex shapes with more control points requires more computational resources. (3) *Scalability*: The method demonstrates scalability as the number of primitives increases. Despite the increase in computational cost, the time cost per epoch remains within a reasonable range, indicating that the method can handle larger scenes with a manageable increase in computational resources.

Overall, although the average time cost per epoch increases with the arise of primitive scale and complexity, our method demonstrates scalability without a significant increase in time cost per epoch.

# of Primitives	Primitive Complexity		Avg. Time Cost per Epoch (s)
	Low (s)	High (s)	
50	0.42	0.71	0.56
100	0.66	1.39	1.02
200	1.14	2.32	1.73
400	2.68	3.69	3.19
600	3.99	4.68	4.34
800	5.02	5.34	5.18
1000	5.68	5.83	5.75

Table 1: Average time cost per epoch for different numbers of primitives and complexity levels.

Convergence By monitoring the loss values over time, we assessed the convergence speed and stability of our approach for different numbers of primitives and complexity levels. As Figure 6 shows, our method consistently converges to a low overall loss of around 100 epochs. Taking the average time cost per epoch in various cases, time consumed for a general collage optimization can be estimated from 1 minute (with 50 visual primitives) to 10 minutes (with 1000 visual primitives).

In our study, we focused on primitive shapes without complex boundaries which could make the iterations converge rapidly. It is important to note that complex primitive shapes have the potential to introduce variations in the convergence epochs. Table 2 provides the information of examples generated in this work. As can be seen here, it is important

Example	# of Primitives	Time Cost per Epoch (s)	Converge Epoch	Time Cost Total (s)
Fig. 5(i)	100 (765paths)	4.05	250	1014
Fig. 5(d)	200 (200paths)	0.579	2030	1175
Fig. 5(f)	200 (400paths)	2.263	350	792
Fig. 4(b)	71 (71paths)	0.495	600	297
Fig. 4(c)	71(142paths)	1.604	730	1171

Table 2: Time cost for examples in this work.

to acknowledge the need for further investigation into the specific impact of primitive complexity on convergence epochs. This aspect could be explored in future research endeavors.

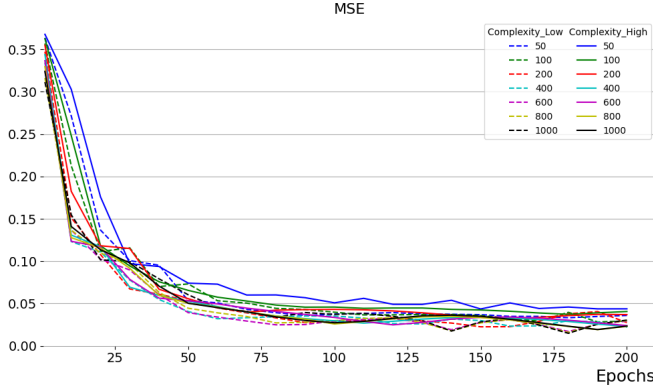


Fig. 6: MSE loss values changing over iterations

6.2 Data Encoding Fidelity

As introduced in Section 4.3, there is no data encoding loss if the scale of all visual primitives is uniform, namely a global scale to all visual primitives. In this section, we report the results of evaluating our methods based on data encoding fidelity, when primitives are scaled individually and constrained by the data fidelity loss.

Figure 7 illustrates the change in data fidelity loss over iterations. On average, the convergence of the loss occurs around 350 epochs, regardless of the number of primitives. As the number of primitives increases, there is a slight increase in the data fidelity loss. This observation can be attributed to the increased difficulty in maintaining correspondence between a larger number of primitives and the raw data.

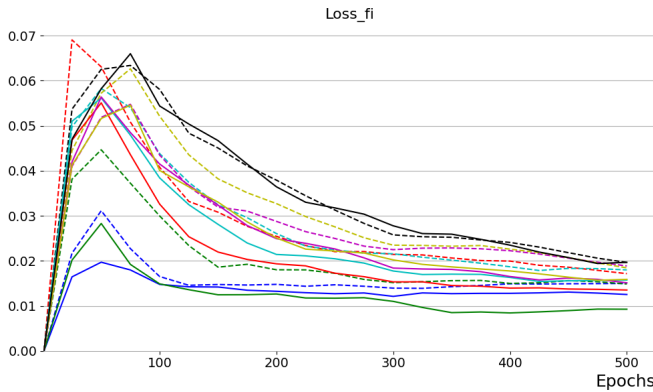


Fig. 7: Data fidelity loss changing over iterations

We tested on different weight γ of data fidelity loss in the optimization, results in different encoding errors. Here, the encoding errors is computed as the average corresponding difference between every pair of data items in the visualization. A clear negative correlation between

the weight and loss can be observed: with a small weight ($=1e5$ in our study), the encoding error can be around $\pm 3.0\%$, with a larger weight ($=1e8$), the encoding error can be reduced to $\pm 0.4\%$.

Our framework offers customization options to cater to different requirements on data fidelity. When dealing with visualizations that demand high encoding precision, such as a Square Map depicting 100 companies in the USA (left-top one in Figure 1), we have two approaches. One is, we can employ a global scale transformation on the primitives to ensure accurate representation. Alternatively, we can employ individual scale transformation, and constrain the optimization problem by assigning a large weight to the data fidelity loss term. This weight emphasizes the importance of preserving the fidelity of the underlying data during the optimization process.

Conversely, if a visualization has a more relaxed requirement on data encoding precision, we can assign a smaller weight to the data fidelity loss. This flexibility allows to strike a balance between fidelity and other optimization objectives. However, it is important to note that a large weight on the fidelity loss may negatively impact the optimization of the other two losses, namely the smoothness and boundary losses. For instance, in the case of USA map visualization, applying a large weight to the data fidelity loss might result in overlapping rectangles.

7 SUMMARY, LIMITATIONS AND FUTURE WORK

In this work, we have introduced a novel approach to creating collage visualizations by leveraging vector graphics manipulation through an optimization process aimed at minimizing loss in image space. Through the diverse examples presented in Section 5, we have demonstrated the versatility of our method in generating visually compelling collages, while maintaining fidelity to the underlying data. Our image-space approach empowers users to explore their creativity, experiment with novel visual elements, and incorporate imaginative concepts, thereby expanding the possibilities for expressive and engaging visualizations.

In the following, we delve and discuss the limitations of our method, addressing areas where improvements can be made.

Packing Quality In our experiment, we learned that when the visual primitives are not limited by data encoding fidelity, we can achieve high-quality packing results. This means that the packing, as shown in Figure 5 with the example of wine, has minimal overlap and is compact. However, when we introduce data fidelity constraints, there may be some overlapping among visual primitives, as observed in the USA map depicted in Figure 1. In such cases, our packing quality may not be as good as that achieved by specialized tools like *ShapeWordle* [32] for a wordle application. Furthermore, the packing quality of icons is inferior to that of specialized geometric descriptors [14]. Hence, for future research, a promising direction would involve combining image-space collage techniques as a solid foundation, supplemented by a few optimization steps in the object-space to enhance the packing rate. This compound methodology has the potential to yield significant improvements in the tradeoff between speed and quality.

Shadow Trap During the optimization process, it is possible to encounter situations where a primitive becomes immobilized due to being fully obstructed or covered by other primitives. As depicted in Figure 8, some small primitives are surrounded, rendering them unable to freely adjust and fit into their surroundings. This obstruction leads to a state of stagnation, where the primitive remains stationary and unable to move. To address this issue, a potential solution for overcoming the ‘‘shadow trap’’ could involve implementing intelligent algorithms that detect and prevent the complete coverage of primitives. By incorporating adaptive strategies or dynamic rearrangement techniques, future research could aim to enhance the object’s ability to navigate its surroundings and avoid getting trapped.

Primitive Seeding In our study, we experimented with a MAT-based method for assigning primitives by considering their sizes and placing them along median axes. This approach proves highly effective for shapes with varying widths, including tubes and necks, as seen in the shape ‘@’ and ‘tail of seahorse’ in Figure 5. Our experiments validate the promising results achieved through this initialization technique. However, it is important to note that while our MAT-based method succeeds for certain shapes, it may not be optimal for others. For

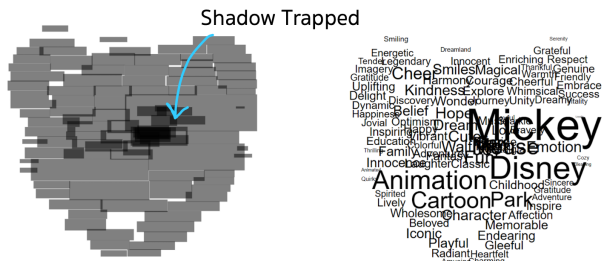


Fig. 8: Shadow Trap in Optimization: primitive becomes immobilized due to being fully obstructed or covered by other primitives.

instance, when dealing with round bellies, an alternative approach like random sampling can be more suitable and effective. A well-chosen initialization contributes significantly to accurate and efficient shape representation. Therefore, further research efforts is required to develop intelligent seeding techniques that automatically suggest or generate initial visual primitives based on the underlying data characteristics. This would streamline the visualization creation process and provide users with a warm start for their designs.

In light of the advancements made, there are several promising directions for future research and development. One potential avenue is the exploration of interactive interfaces for target image-space editing in visualization creation. By providing users with intuitive editing and controls in the target image, they can directly manipulate and refine the visual elements in return, allowing for a more interactive and iterative design process. A more concrete avenue can use text-driven editing based on a text-to-image foundation model [9] [11].

REFERENCES

- [1] M. Bostock, V. Ogievetsky, and J. Heer. D³ data-driven documents. *IEEE transactions on visualization and computer graphics*, 17(12):2301–2309, 2011. 2
- [2] M.-T. Chi, S.-S. Lin, S.-Y. Chen, C.-H. Lin, and T.-Y. Lee. Morphable word clouds for time-varying text data visualization. *IEEE transactions on visualization and computer graphics*, 21(12):1415–1426, 2015. 2
- [3] W. Cui, Y. Wu, S. Liu, F. Wei, M. X. Zhou, and H. Qu. Context preserving dynamic word cloud visualization. In *2010 IEEE Pacific Visualization Symposium (PacificVis)*, pp. 121–128. IEEE, 2010. 2
- [4] S. Goferman, A. Tal, and L. Zelnik-Manor. Puzzle-like collage. In *Computer graphics forum*, vol. 29, pp. 459–468. Wiley Online Library, 2010. 2
- [5] M. A. Hearst, E. Pedersen, L. Patil, E. Lee, P. Laskowski, and S. Francneri. An evaluation of semantically grouped word cloud designs. *IEEE transactions on visualization and computer graphics*, 26(9):2748–2761, 2019. 2
- [6] C.-Y. Hsu, L.-Y. Wei, L. You, and J. J. Zhang. Autocomplete element fields. In *Proceedings of the 2020 CHI Conference on Human Factors in Computing Systems*, pp. 1–13, 2020. 2
- [7] H. Huang, L. Zhang, and H.-C. Zhang. Arcimboldo-like collage using internet images. In *Proceedings of the 2011 SIGGRAPH Asia Conference*, pp. 1–8, 2011. 2
- [8] S. Huron, R. Vuillemot, and J.-D. Fekete. Visual sedimentation. *IEEE Transactions on Visualization and Computer Graphics*, 19(12):2446–2455, 2013. 4
- [9] S. Iluz, Y. Vinker, A. Hertz, D. Berio, D. Cohen-Or, and A. Shamir. Word-as-image for semantic typography. *ACM Transactions on Graphics (TOG)*, 42(4):1–11, 2023. 8
- [10] T. Itoh, Y. Yamaguchi, Y. Ikehata, and Y. Kajinaga. Hierarchical data visualization using a fast rectangle-packing algorithm. *IEEE Transactions on Visualization and Computer Graphics*, 10(3):302–313, 2004. 1, 2
- [11] A. Jain, A. Xie, and P. Abbeel. Vectorfusion: Text-to-svg by abstracting pixel-based diffusion models. In *Proceedings of the IEEE/CVF Conference on Computer Vision and Pattern Recognition*, pp. 1911–1920, 2023. 8
- [12] J. Jo, B. Lee, and J. Seo. Wordleplus: expanding wordle’s use through natural interaction and animation. *IEEE computer graphics and applications*, 35(6):20–28, 2015. 2
- [13] K. Koh, B. Lee, B. Kim, and J. Seo. Maniwordle: Providing flexible control over wordle. *IEEE Transactions on Visualization and Computer Graphics*, 16(6):1190–1197, 2010. 2
- [14] K. C. Kwan, L. T. Sinn, C. Han, T.-T. Wong, and C.-W. Fu. Pyramid of arclength descriptor for generating collage of shapes. *ACM Trans. Graph.*, 35(6):229–1, 2016. 1, 2, 7
- [15] D.-T. Lee. Medial axis transformation of a planar shape. *IEEE Transactions on pattern analysis and machine intelligence*, (4):363–369, 1982. 3
- [16] G. Lee, M. Kim, Y. Lee, M. Lee, and B.-T. Zhang. Neural collage transfer: Artistic reconstruction via material manipulation. In *Proceedings of the IEEE/CVF International Conference on Computer Vision*, pp. 2394–2405, 2023. 2
- [17] C. Li, X. Dong, and X. Yuan. Metro-wordle: An interactive visualization for urban text distributions based on wordle. *Visual Informatics*, 2(1):50–59, 2018. 2
- [18] T.-M. Li, M. Lukáč, M. Gharbi, and J. Ragan-Kelley. Differentiable vector graphics rasterization for editing and learning. *ACM Transactions on Graphics (TOG)*, 39(6):1–15, 2020. 1, 2
- [19] L. Liu, H. Zhang, G. Jing, Y. Guo, Z. Chen, and W. Wang. Correlation-preserving photo collage. *IEEE transactions on visualization and computer graphics*, 24(6):1956–1968, 2017. 2
- [20] S. Liu, J. Yin, X. Wang, W. Cui, K. Cao, and J. Pei. Online visual analytics of text streams. *IEEE transactions on visualization and computer graphics*, 22(11):2451–2466, 2015. 2
- [21] R. Maharik, M. Bessmeltsev, A. Sheffer, A. Shamir, and N. Carr. Digital micrography. *ACM Transactions on Graphics (TOG)*, 30(4):1–12, 2011. 2
- [22] C. McNaught and P. Lam. Using wordle as a supplementary research tool. *Qualitative Report*, 15(3):630–643, 2010. 2
- [23] X. Pan, F. Tang, W. Dong, C. Ma, Y. Meng, F. Huang, T.-Y. Lee, and C. Xu. Content-based visual summarization for image collections. *IEEE transactions on visualization and computer graphics*, 27(4):2298–2312, 2019. 2
- [24] F. V. Paulovich, F. M. Toledo, G. P. Telles, R. Minghim, and L. G. Nonato. Semantic wordification of document collections. In *Computer Graphics Forum*, vol. 31, pp. 1145–1153. Wiley Online Library, 2012. 2
- [25] A. W. Rivadeneira, D. M. Gruen, M. J. Muller, and D. R. Millen. Getting our head in the clouds: toward evaluation studies of tagclouds. In *Proceedings of the SIGCHI conference on Human factors in computing systems*, pp. 995–998, 2007. 2
- [26] C. Rother, L. Bordeaux, Y. Hamadi, and A. Blake. Autocollage. *ACM transactions on graphics (TOG)*, 25(3):847–852, 2006. 2
- [27] T. Surazhsky and G. Elber. Artistic surface rendering using layout of text. In *Computer Graphics Forum*, vol. 21, pp. 99–110. Wiley Online Library, 2002. 2
- [28] O. Van Kaick, H. Zhang, G. Hamarneh, and D. Cohen-Or. A survey on shape correspondence. In *Computer graphics forum*, vol. 30, pp. 1681–1707. Wiley Online Library, 2011. 1
- [29] F. B. Viegas, M. Wattenberg, and J. Feinberg. Participatory visualization with wordle. *IEEE transactions on visualization and computer graphics*, 15(6):1137–1144, 2009. 1, 2
- [30] J. Wang, L. Quan, J. Sun, X. Tang, and H.-Y. Shum. Picture collage. In *2006 IEEE Computer Society Conference on Computer Vision and Pattern Recognition (CVPR’06)*, vol. 1, pp. 347–354. IEEE, 2006. 2
- [31] W. Wang, H. Wang, G. Dai, and H. Wang. Visualization of large hierarchical data by circle packing. In *Proceedings of the SIGCHI conference on Human Factors in computing systems*, pp. 517–520, 2006. 1, 2
- [32] Y. Wang, X. Chu, K. Zhang, C. Bao, X. Li, J. Zhang, C.-W. Fu, C. Hurter, O. Deussen, and B. Lee. Shapewordle: tailoring wordles using shape-aware archimedean spirals. *IEEE Transactions on Visualization and Computer Graphics*, 26(1):991–1000, 2019. 1, 2, 7
- [33] Y. Wu, T. Provan, F. Wei, S. Liu, and K.-L. Ma. Semantic-preserving word clouds by seam carving. In *Computer Graphics Forum*, vol. 30, pp. 741–750. Wiley Online Library, 2011. 2
- [34] L. Xie, X. Shu, J. C. Su, Y. Wang, S. Chen, and H. Qu. Creating emordle: Animating word cloud for emotion expression. *IEEE Transactions on Visualization and Computer Graphics*, 2023. 2
- [35] J. Xu and C. S. Kaplan. Calligraphic packing. In *Proceedings of Graphics Interface 2007*, pp. 43–50, 2007. 2
- [36] X. Xu, L. Zhang, and T.-T. Wong. Structure-based ascii art. In *ACM SIGGRAPH 2010 papers*, pp. 1–10, 2010. 2
- [37] J. Zhang, Z. Yang, L. Jin, Z. Lu, and J. Yu. Creating word paintings jointly

considering semantics, attention, and aesthetics. *ACM Transactions on Applied Perceptions (TAP)*, 19(3):1–21, 2022. 2

- [38] J. Zhao, N. Cao, Z. Wen, Y. Song, Y.-R. Lin, and C. Collins. # fluxflow: Visual analysis of anomalous information spreading on social media. *IEEE transactions on visualization and computer graphics*, 20(12):1773–1782, 2014. 2
- [39] C. Zou, J. Cao, W. Ranaweera, I. Alhashim, P. Tan, A. Sheffer, and H. Zhang. Legible compact calligrams. *ACM Transactions on Graphics (TOG)*, 35(4):1–12, 2016. 2